



The effect of processing additive on aggregated fullerene derivatives in bulk-heterojunction polymer solar cells

Jung Hwa Seo^a, Sun Young Nam^b, Kwang-Sup Lee^{b,*}, Tae-Dong Kim^b, Shinuk Cho^{c,*}

^a Department of Materials Physics, Dong-A University, Busan 604-714, Republic of Korea

^b Department of Advanced Materials, Hannam University, Daejeon 305-811, Republic of Korea

^c Department of Physics and EHSRC, University of Ulsan, Ulsan 680-749, Republic of Korea

ARTICLE INFO

Article history:

Received 21 October 2011

Received in revised form 26 December 2011

Accepted 28 December 2011

Available online 15 January 2012

Keywords:

Processing additives

Fullerene derivatives

Field-effect transistors

Polymer solar cells

Nano-scale morphology

ABSTRACT

The effects of processing additive on fullerene aggregation in polymer BHJ solar cells were investigated using new fullerene derivatives bearing a thiophene moiety and alkyl groups. Although new fullerene derivatives showed quite similar electronic transport properties in field-effect transistors, the photovoltaic performances were significantly limited by their aggregative nature. Processing with 1% CN additive, however, changed the aggregated morphology of BHJ films to a smoother and homogeneous morphology, improving photovoltaic performance. The result indicates that processing additive not only influences on polymer side, but also significantly affects fullerene acceptor component.

© 2012 Elsevier B.V. All rights reserved.

1. Introduction

Bulk heterojunction (BHJ) solar cells have generated strong interest in the field of renewable energy because of their potential to lower manufacturing costs for large-area and lightweight devices [1–3]. Considerable effort has been expended to improve the power conversion efficiency (PCE) by means of new materials design, interface control, and device fabrication [4–8]. Process engineering via thermal annealing, solvent annealing, and solvent additives have been utilized to significantly enhance device performance of these BHJ solar cells [9–11].

One of key factors governing the PCEs is the nano-scale morphology of the blend comprising conjugated polymer donors and fullerene acceptors [9–12]. A desired morphology plays a critical role affecting interfaces for charge separation of photogenerated excitons and continuous pathway for separated charge carrier transport. In 2006, solvent additives were found to be a particularly effective way to influence on the phase separation during film for-

mation [13–16]. This processing additive method is simple and amenable to solution deposition methods and does not require post processing modification such as thermal annealing or solvent annealing.

Two types of processing additive have been used to control nano-scale morphology of BHJ solar cells. One is the method using selective solubility of additive. This type processing additive, such as 1,8-octanedithiol and 1,8-diodooctane, leads to aggregation of the ‘polymer’ in solution, which results in an increase in the size of the BHJ domains in the film [13,14,17]. The effect of additive using selective solubility, therefore, highly depends on the tendency of polymer to aggregate. This type additive does not effectively work on the high aggregative polymer systems.

A second type of cosoluble additive, 1-chloronaphthalene (CN), has been used in BHJ materials comprising aggregative conjugated polymer donors [15,16]. By using the cosoluble additive, large-scale aggregation of polymer is suppressed and the nanoscale morphology required for high-performance BHJ is achieved.

The use of processing additives in the optimization of the nanoscale morphology of BHJ films has been shown to be effective in many systems. However, the effects of

* Corresponding authors.

E-mail addresses: kslee@hnu.kr (K.-S. Lee), sucho@ulsan.ac.kr (S. Cho).

processing additives are yet to be fully explored on fullerene acceptor side. In this contribution, we have investigated the effect of additive focused on acceptor side.

2. Experimental

2.1. Materials

The synthetic procedure of C₆₀-fused N-methyl-2-(3-hexylthiophen-2-yl)pyrrolidine (C₆₀ThHx) was previously reported in the literature [18,19]. The synthetic approach for C₆₀-fused N-methyl-2-(3-octylthiophen-2-yl)pyrrolidine (C₆₀ThOt) is depicted in Scheme 1. All reagents were purchased from commercial sources and used without further purification unless otherwise noted. All solvents were purified and freshly distilled prior to use according to literature procedures.

2.1.1. Synthesis of 3-octylthiophene (1)

A solution containing thiophene (0.10 mol) in dry THF (120 mL) at –78 °C was treated with 1.6 M of *n*-BuLi (0.12 mol) in hexane and stirred for 1 h. 1-Bromooctane (0.12 mol) in dry THF (20 mL) was slowly added in the solution at –78 °C and the solution was allowed to warm to RT and stirred overnight. The solution was quenched with a saturated NH₄Cl solution and extracted with ether. The combined ether extracts were washed with brine, dried over MgSO₄, filtered and concentrated under reduced pressure. The resulting crude product was purified by a flash chromatography on silica gel with an eluent of hexane to give of compound **1** (yield: 80%). ¹H NMR (CDCl₃, TMS, ppm): δ 7.07 (d, 1H), 6.86 (t, 1H), 6.73 (d, 1H), 2.81 (t, 2H), 1.69 (m, 2H), 1.30 (m, 10H), 0.83 (t, 3H).

2.1.2. Synthesis of 2-bromo-3-octylthiophene (2)

To a solution of 3-octylthiophene (0.05 mol) and 120 mL acetic acid, NBS (0.06 mol) was added in one portion and stirred for 30 min. And then water was added into the resulting solution, and also stirred for 10 min. The mixture was

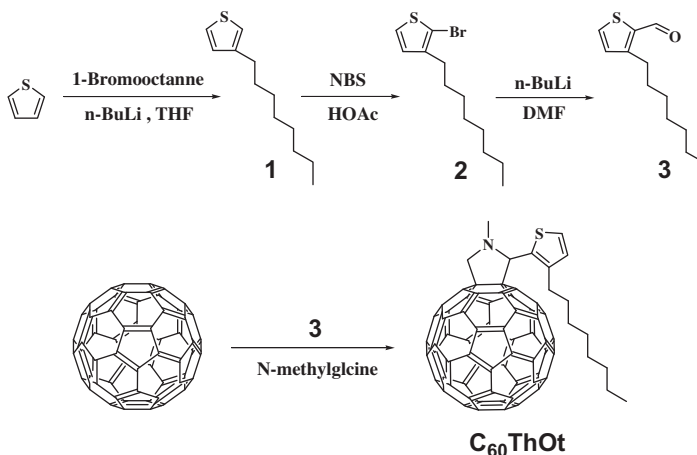
washed with ether, saturated aqueous NaHCO₃, and water, and dried with MgSO₄. The solvent was removed via rotary evaporation, and 2-bromo-3-octylthiophene (yield: 86%) was obtained. ¹H NMR (CDCl₃, TMS, ppm): δ (ppm) 7.17 (d, 1H), 6.80 (d, 1H), 2.59 (t, 2H), 1.60 (m, 2H), 1.35 (m, 10H), 0.93 (t, 3H).

2.1.3. Synthesis of 3-octylthiophene-2-carbaldehyde (3)

Butyllithium (0.024 mol, 1.6 M in hexane) was added to a stirred solution of 2-bromo-3-octylthiophene (0.02 mol) in THF (25 mL) at –78 °C and the resulting solution was stirred for 15 min. Then, dimethylformamide (0.04 mol) was added and the resulting solution was left to reach room temperature and stirred for additional 30 min at room temperature. An aqueous saturated solution of NH₄Cl (25 mL) was then added to the reaction mixture and the organic layer was separated. The aqueous layer was extracted with diethyl ether, the combined organic extracts were dried (Na₂SO₄), the solvent was removed in the rotary evaporator, and the resulting residue was purified by flash chromatography (yield: 70%). ¹H NMR (CDCl₃, TMS, ppm): δ (ppm) 10.04 (s, 1H), 7.64 (d, 1H), 7.00 (d, 1H), 2.96 (t, 2H), 1.74 (m, 2H), 1.66 (m, 10H), 0.87 (t, 3H).

2.1.4. Synthesis of C₆₀ThOt

A solution of **3** (0.09 mol), fullerene (0.09 mol), and *N*-methylglycine (0.20 mol) in 1,2-dichlorobenzene (30 mL) was refluxed for 48 h. After cooling to RT, the reaction mixture was performed with a flash chromatography on silica gel with a gradient eluent of toluene to 20% hexane in toluene. After the crude product was washed and centrifuged with methanol, recrystallization from 1,4-dioxane yielded the desired product C₆₀ThOt (yield: 40%). ¹H NMR (CDCl₃, TMS, ppm): δ 7.18 (d, 1H), 6.92 (d, 1H), 5.19 (s, 1H), 5.00 (d, 1H), 4.23 (d, 1H), 2.89 (s, 3H), 2.05 (t, 2H), 1.60 (m, 2H), 1.32 (m, 10H), 0.85 (t, 3H). MALDI-TOF-MS (matrix, 2,5-dihydroxybenzoic acid (2,5-DHB)): calcd for C₇₅H₂₅NS 972.07; found 973.09 [M⁺].



Scheme 1. Synthetic routes for C₆₀ThOt.

2.2. Characterizations

2.2.1. Absorption measurements

Absorption measurements were measured using a Beckman Coulter DU800 spectrometer. Solutions of bare PCBM and fullerene derivatives were prepared in chloroform with the concentration of 5 mg/mL were spin cast on pre-cleaned glass substrates.

2.2.2. Ultraviolet photoelectron spectroscopy

70 nm thick Au film was deposited on pre-cleaned Si substrates with a thin native oxide. Solutions of bare PCBM, C₆₀ThHx and C₆₀ThOt in chloroform, 0.2% (w/v) were spin cast at spin speed of 2000 rpm for 40 s. All films were fabricated inside a N₂-glovebox and were transferred via an airtight sample holder to the UPS analysis chamber. Samples were also kept in a high vacuum chamber overnight to remove solvent residues. The UPS chamber was equipped with a hemispherical electron energy detector (Kratos Ultra Spectrometer) and was maintained at 1×10^{-9} torr. The UPS measurements were carried out using the He I ($h\nu = 21.2$ eV) source. During UPS measurements, a sample bias of -9 V was used in order to separate the sample and the secondary edge for the analyzer.

2.2.3. Field-effect transistors

All OFETs were fabricated on heavily n-type doped Si wafers with a 200 nm thick thermally grown SiO₂ layer. The n-type doped Si substrate functioned as the gate electrode and the SiO₂ layer functioned as the gate dielectric. Bare PCBM, C₆₀ThHx and C₆₀ThOt solutions in chloroform, 0.5% (w/v) were spin cast with the spin speed of 2000 rpm for 40 s. The film thickness was approximately 60 nm. All deposition was carried out in N₂-glovebox. 100 nm thick Al electrodes were deposited by thermal evaporation using a shadow mask. Channel length (L) and channel width (W) were 50 μm and 3.45 mm, respectively. Electrical characterization was performed under N₂ atmosphere using a Keithley 4200 semiconductor parametric analyzer.

2.2.4. Bulk heterojunction solar cells

Polymer solar cells were fabricated using Si-PCPDTBT as the donor and PCBM, C₆₀ThHx and C₆₀ThOt as the acceptors. The ITO-coated glass substrates were cleaned with detergent, distilled water, acetone, and isopropyl alcohol in an ultrasonic bath and the dried overnight in an oven at >100 °C. After UV ozone treatment of the ITO substrates for 20 min, 40 nm thick PEDOT:PSS layer was spin-cast from aqueous solution (5000 rpm for 40 s). The substrates were dried at 140 °C for 10 min in air and transferred to a N₂-glovebox for spin-casting the blend layers. The blend solutions of Si-PCPDTBT:PCBM (1:2 w/v), Si-PCPDTBT:C₆₀ThHx (1:2 w/v) and Si-PCPDTBT:C₆₀ThOt (1:2 w/v) in 1,2-dichlorobenzene (concentration of 7 mg/mL) were prepared without or with 1 vol.% CN by volume. The thickness of blend layers were average 100 nm (from 2000 rpm for 40 s) measured by profilometer. The ultra-thin PFN⁺Blm₄ layer was subsequently deposited by spin-casting from 0.02% (w/v) solution in methanol [7,20,21]. The final step in device construction involves thermal evaporation of 100 nm thick Al electrodes. Current–voltage characteristic

curves were measured using a Keithley 2400 source meter. The device area was 9.84 mm² with using an aperture. All data were obtained under AM 1.5G illumination from a calibrated solar simulator with irradiation intensity of 100 mW cm⁻² under ambient atmosphere. EQE spectra were measured using a solar cell spectral response/QE/IPCE measurement system (PV Measurements Inc., Model QE W 7).

2.2.5. DFT calculations

DFT calculations were performed using the Gaussian 03 package with the nonlocal hybrid Becke three-parameter Lee–Yang–Parr (B3LYP) function and the 6-31G* basis set to obtain the HOMO and LUMO levels after optimizing the geometry of materials using the same method.

2.2.6. Atomic force microscopy

Tapping mode AFM images were collected under N₂-atmosphere using the Nanoscope III controller (Veeco). Silicon probes with spring constants of 5 N/m and resonant frequencies of 75 kHz were used.

3. Results and discussion

Three different fullerene derivatives, [6,6]-phenyl-C₆₁-butyric acid methyl ester (PCBM), C₆₀-fused N-methyl-2-(3-hexylthiophen-2-yl)pyrrolidine (C₆₀ThHx), and C₆₀-fused N-methyl-2-(3-octylthiophen-2-yl)pyrrolidine (C₆₀ThOt), are used as the acceptor materials, whose molecular structures are shown in Fig. 1. As an donor material for solar cell, a narrow gap polymer, poly[(4,4'-bis(2-ethylhexyl)dithiene [3,2-b:2',3'-d]silole)-2,6-diyl-*alt*-(4,7-bis(2-thienyl)-2,1,3-benzothiadiazole)-5,5'-diyl] (Si-PCPDTBT) are used.

The UV–vis absorption spectra of pristine PCBM, C₆₀ThHx, C₆₀ThOt and Si-PCPDTBT thin films are shown in Fig. 2(a) for comparison. The absorptions centered in the range of 300–600 nm for C₆₀ThHx and C₆₀ThOt are more intense than that of PCBM in the same range of wavelengths. The optical gaps of PCBM, C₆₀ThHx and C₆₀ThOt were extracted 1.7 eV, 1.50 eV, and 1.55 eV, respectively.

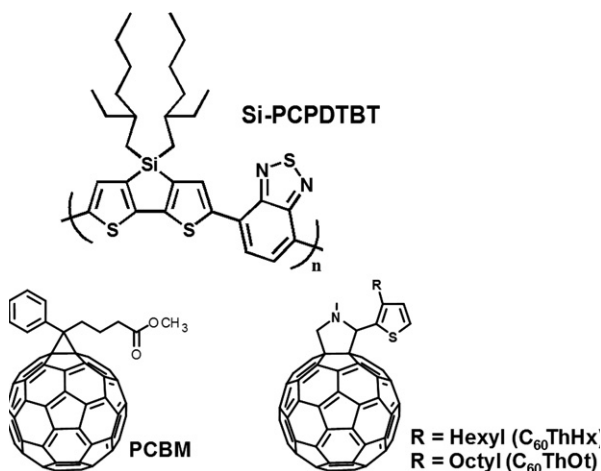


Fig. 1. Chemical structures of materials studied in this work.

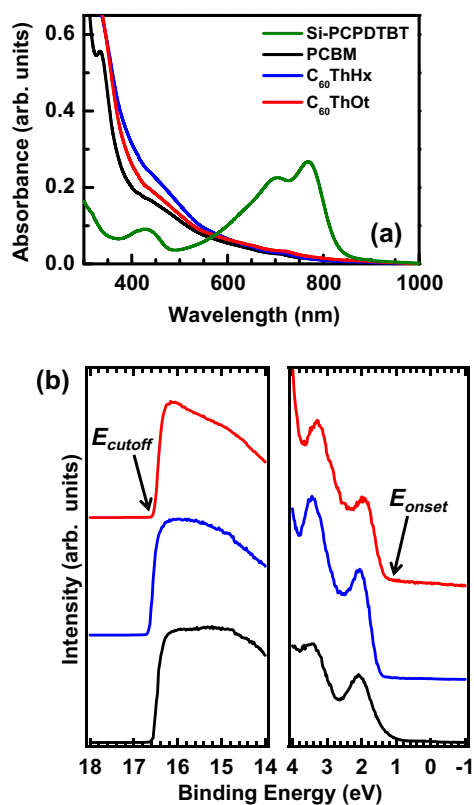


Fig. 2. (a) Absorbance spectra of pristine PCBM, C₆₀ThHx, C₆₀ThOt and Si-PCPDTBT thin films. (b) UPS spectra of PCBM, C₆₀ThHx, and C₆₀ThOt films on Au surface.

As expected, the decreased optical gaps arise from the lower symmetry. The energy of the HOMO can be measured by ultraviolet photoelectron spectroscopy (UPS) and that of the LUMO by subtracting the value of the optical gap (obtained from Fig. 2(b)) in which the HOMO was calculated from the binding energy in the solid state and the LUMO was estimated using the optical gap of the films. Fig. 2(b) shows the high binding energy cutoff (14–18 eV) and the HOMO region (0–4 eV) of UPS spectra taken from pristine PCBM, C₆₀ThHx and C₆₀ThOt thin films on Au surfaces. The abscissa is the binding energy relative to the Fermi level of Au, which is defined by the electron energy before excitation relative to the vacuum level. The HOMO energy is determined by the following equation,

$$E_{HOMO} = h\nu - (E_{cutoff} - E_{onset}) \quad (1)$$

where $h\nu$ is the incident energy of 21.2 eV, the E_{cutoff} and E_{onset} are a turning point from Fig. 2(b), respectively. The resulting HOMO values are 5.95 eV for PCBM, 6.06 eV for C₆₀ThHx and 6.01 eV for C₆₀ThOt within the error range of ± 0.03 eV. The values of the HOMO, LUMO and optical gap are summarized in Table 1. Table 1 also contains theoretical results from the DFT calculations (see Fig. 3) for comparison and FET performance which will be discussed subsequently, so that relative comparisons can be readily made. Despite of uncertainty of the LUMO energy

by exciton binding energy, the HOMO and LUMO energies of PCBM are consistent with reported values [22–24].

Films of each derivative were prepared and found to exhibit fairly different aggregation tendency. Fig. 4 show atomic force microscopy (AFM) images of PCBM, C₆₀ThHx and C₆₀ThOt films on bare SiO₂ measured under an inert N₂ atmosphere. The PCBM surface is relatively smooth and homogenous with root-mean-square (rms) of 0.69 nm. In the case of the C₆₀ThHx, uneven and somewhat aggregate features with rms of 2.03 nm are observed. For the C₆₀ThOt, AFM images show an aggregated morphology surrounded by lobe like features with rms of 4.68 nm.

Interestingly, although the C₆₀ThHx and C₆₀ThOt films show different aggregated morphology, their electronic properties examined by field-effect transistor (FET) are not significantly changed compared to the PCBM. Fig. 5 shows typical source-drain current (I_{ds}) versus gate voltage (V_{gs}) plots of PCBM, C₆₀ThHx and C₆₀ThOt FETs. The transport characteristic curves are almost identical. Linear plots of $I_{ds}^{1/2}$ versus V_{gs} , deduced from the I_{ds} versus V_{gs} measurements, yielded hole mobilities of $\mu_1 = 0.028$ cm²/V s, $\mu_2 = 0.0093$ cm²/V s, and $\mu_3 = 0.011$ cm²/V s for PCBM (μ_1), C₆₀ThHx (μ_2), and C₆₀ThOt (μ_3), respectively. FET data, including mobilities, on/off ratios (I_{on}/I_{off}), and threshold voltages (V_{th}) obtained from these polymers are listed in Table 1 together with energy level parameters. Output characteristics of C₆₀ThHx and C₆₀ThOt FETs are shown in Fig. 5(b) and (c), respectively. These FET results indicate that, even though the C₆₀ThHx and C₆₀ThOt exhibit aggregative nature, continuous network for charge transport is well established in all materials and their electronic properties are very close.

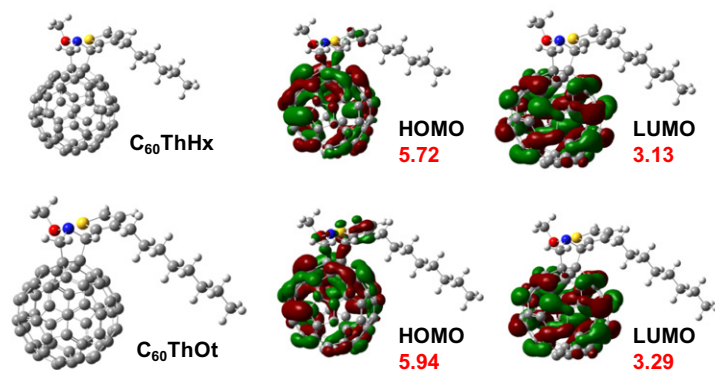
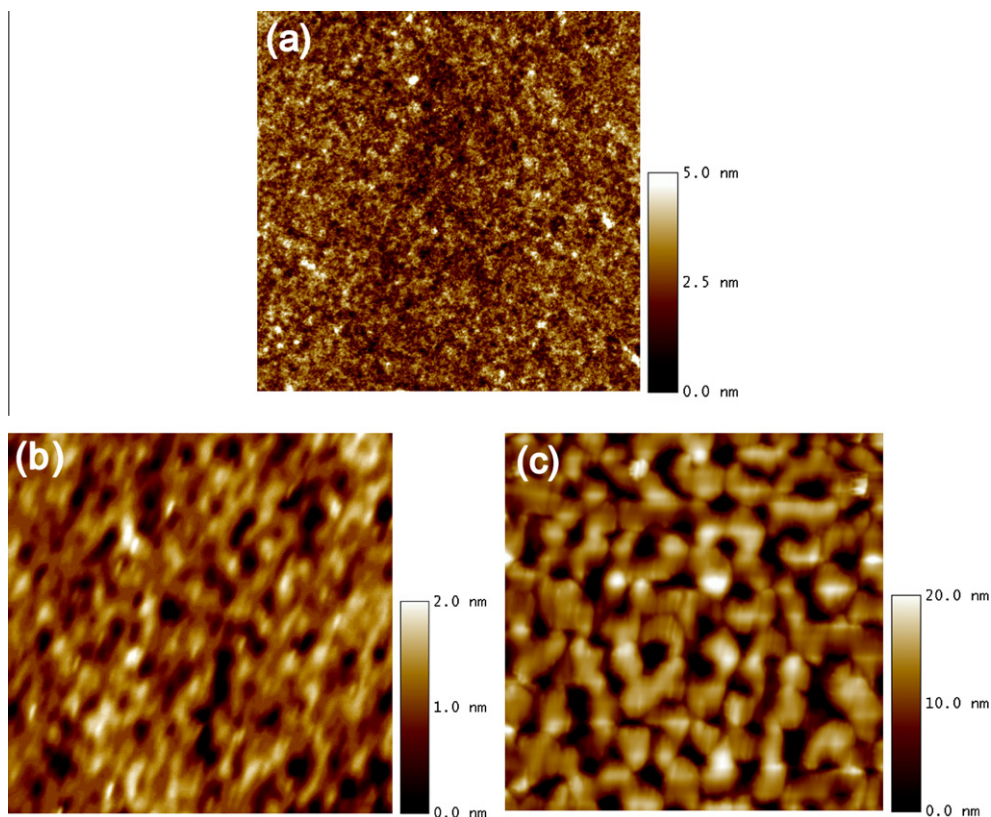
Although no significant problems are encountered in FET devices fabricated using one component system, aggregative tendencies may influence the performance of BHJ solar cells incorporating two components. Fig. 6(a) shows the current density–voltage (J – V) characteristics of BHJ solar cells fabricated using a narrow gap polymer, Si-PCPDTBT and three fullerene derivatives, PCBM, C₆₀ThHx, and C₆₀ThOt. The control device of Si-PCPDTBT:PCBM yields a PCE of 4.45%, short circuit current (J_{sc}) of 13.0 mA/cm², open circuit voltage (V_{oc}) of 0.60 V, and fill factor (FF) of 0.57. Due to the aggregated nature of C₆₀ThHx and C₆₀ThOt, the photovoltaic performance of Si-PCPDTBT:C₆₀ThHx and Si-PCPDTBT:C₆₀ThOt devices are limited compared to the device based on Si-PCPDTBT:PCBM mixture. Si-PCPDTBT:C₆₀ThHx and Si-PCPDTBT:C₆₀ThOt devices exhibit PCE of 3.45%, J_{sc} of 10.8 mA/cm², V_{oc} of 0.61 V, and FF of 0.50, and PCE of 2.38%, J_{sc} of 8.6 mA/cm², V_{oc} of 0.62 V, and FF of 0.42, respectively.

In order to investigate whether the processing additive also can affect the fullerene component like the additive effect on polymer part, we used the cosoluble additive CN (1 vol.%) in BHJ mixtures. Fig. 6(b–d) show the J – V characteristics of solar cell devices with and without CN additive. For the Si-PCPDTBT:PCBM solar cell (Fig. 6(b)), no significant changes are observed. In contrast to the PCBM devices, the introduction of CN led to a small increase in J_{sc} from 10.8 mA/cm² to 11.2 mA/cm² for the Si-PCPDTBT:C₆₀ThHx solar cell (see Fig. 6(c)) and an increase from 8.6 mA/cm² to 9.6 mA/cm² for the Si-PCPDTBT:C₆₀ThOt solar cell (see

Table 1

Energy levels obtained from theoretical and experimental methods, and transistor device parameters.

	Experimental values ^a			Theoretical values ^b			FET performance		
	HOMO (± 0.03 eV)	LUMO (± 0.05 eV)	E_g^{opt} (± 0.05 eV)	HOMO (eV)	LUMO (eV)	E_g (eV)	μ ($\text{cm}^2/\text{V s}$)	V_{th} (V)	I_{on}/I_{off}
PCBM	5.95	4.25	1.70	5.81	3.26	2.55	2.8×10^{-2}	2.5	1×10^6
C ₆₀ ThHx	6.06	4.56	1.50	5.72	3.13	2.59	9.3×10^{-3}	1.6	3×10^5
C ₆₀ ThOt	6.01	4.46	1.55	5.94	3.29	2.65	1.1×10^{-2}	2.2	8×10^5
Si-PCPDTBT	4.8	3.3	1.5	–	–	–	5.1×10^{-3}	4.7	4×10^5

^a HOMO values were determined by UPS, while LUMO values were estimated by subtracting from optical gap (E_g).^b All chemical structures were optimized with the B3LYP function and a basis set of 6-31G*.**Fig. 3.** DFT calculations of C₆₀ThHx and C₆₀ThOt.**Fig. 4.** AFM images ($5 \mu\text{m} \times 5 \mu\text{m}$) of pristine (a) PCBM, (b) C₆₀ThHx and (c) C₆₀ThOt films on bare SiO₂.

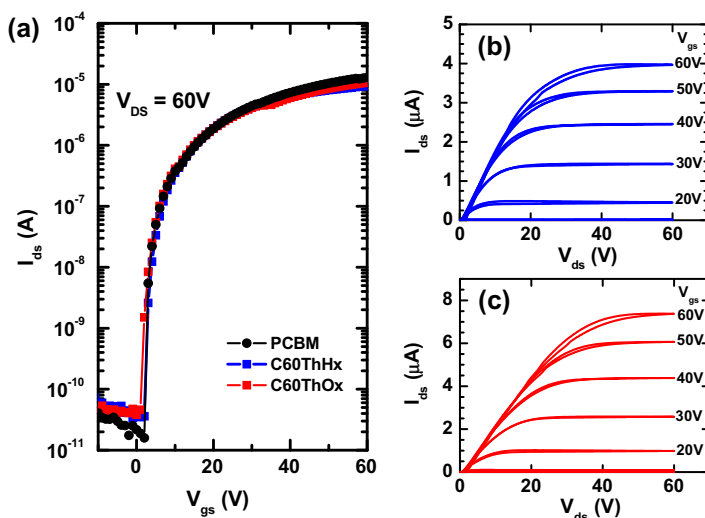


Fig. 5. (a) The transfer characteristics of PCBM, C₆₀ThHx, and C₆₀ThOt FETs on bare SiO₂. Output characteristic curves of (b) C₆₀ThHx FET, and (c) C₆₀ThOt FET.

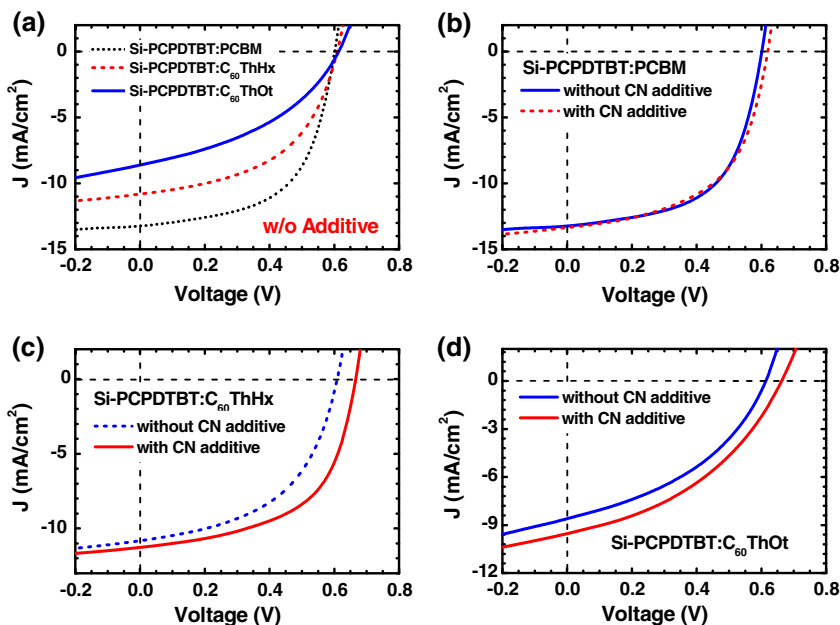


Fig. 6. The J - V characteristics of (a) Si-PCPDTBT:PCBM, Si-PCPDTBT:C₆₀ThHx, and Si-PCPDTBT:C₆₀ThOt solar cells without additive. The J - V characteristics of (b) Si-PCPDTBT:PCBM, (c) Si-PCPDTBT:C₆₀ThHx, (d) Si-PCPDTBT:C₆₀ThOt solar cells with the 1% CN additive.

Fig. 6(d)). Similarly, V_{oc} improved from 0.61 V to 0.67 V for the Si-PCPDTBT:C₆₀ThHx and from 0.62 V to 0.67 V for the Si-PCPDTBT:C₆₀ThOt. FF also improved from 50% to 55% in case of the Si-PCPDTBT:C₆₀ThHx. Consequently, the calculated PCEs increased from 3.29% to 4.13% for the Si-PCPDTBT:C₆₀ThHx and from 2.25% to 2.70% for the Si-PCPDTBT:C₆₀ThOt. The resulting device parameters determined from Fig. 6 are summarized in Table 2.

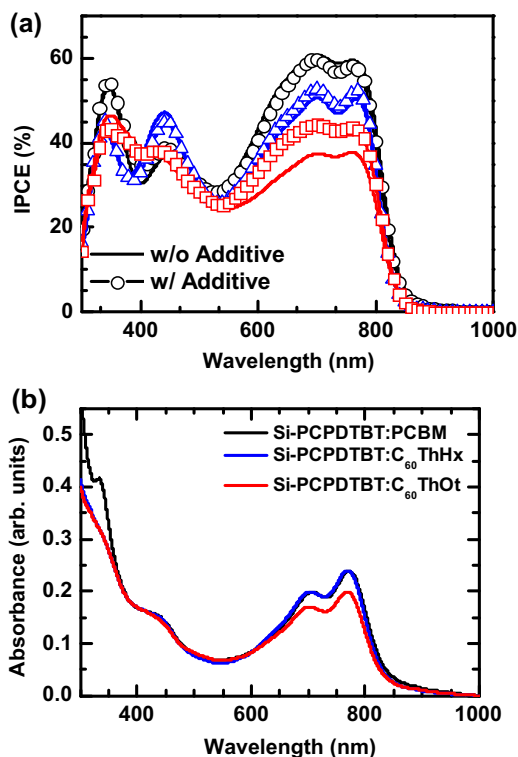
Fig. 7(a) shows the EQE measurement for Si-PCPDTBT:PCBM, Si-PCPDTBT:C₆₀ThHx and Si-PCPDTBT:C₆₀ThOt solar cells. The IPCE intensity of Si-PCPDTBT:PCBM (black trace) was the highest and that of

Si-PCPDTBT:C₆₀ThOt (red trace) was the lowest as shown in Fig. 7(a), consistent with J_{sc} as obtained from the J - V characteristics. The UV-vis absorption spectra of blend thin films were also examined as shown in Fig. 7(b). Comparing the IPCE curves of the devices with the absorption spectra of blend films, the photo-response of devices at 400–900 nm is similar to the corresponding absorption spectra of each blend film. However, since the absorption intensities of Si-PCPDTBT:PCBM and Si-PCPDTBT:C₆₀ThHx are almost identical, the decreased IPCE in the Si-PCPDTBT:C₆₀ThHx device is attributed to a reduction in the probability of carrier collection. In addition, the rel-

Table 2

Device performance of solar cells.

	J_{sc} [mA/cm ²] (<i>J</i> - <i>V</i>)	J_{sc} [mA/cm ²] (IPCE) ^a	V_{oc} (V)	<i>FF</i> (%)	PCE (%) (<i>J</i> - <i>V</i>)	PCE (%) (IPCE) ^a
Si-PCPDTBT/PCBM	13.0	13.0	0.60	0.57	4.45	4.44
Si-PCPDTBT/PCBM, CN	13.2	13.0	0.62	0.54	4.42	4.35
Si-PCPDTBT/C ₆₀ ThHx	10.8	11.3	0.61	0.50	3.29	3.45
Si-PCPDTBT/C ₆₀ ThHx, CN	11.2	11.5	0.67	0.55	4.13	4.24
Si-PCPDTBT/C ₆₀ ThOt	8.6	9.1	0.62	0.42	2.25	2.38
Si-PCPDTBT/C ₆₀ ThOt, CN	9.6	10.1	0.67	0.42	2.70	2.84

^a IPCE results are in Fig. 7.**Fig. 7.** (a) IPCE measurements, (b) normalized absorbance of blend films obtained from CN/dichlorobenzene.

atively low absorption intensity of Si-PCPDTBT:C₆₀ThOt is consistent with the IPCE result.

The influence of CN on surface morphology was investigated by AFM. AFM images (size: 2 μm × 2 μm) taken from Si-PCPDTBT:PCBM, Si-PCPDTBT:C₆₀ThHx and Si-PCPDTBT:C₆₀ThOt devices, shown in Fig. 8(a) and (c), reveal obvious differences in the surface morphologies. The surface of Si-PCPDTBT:PCBM is relatively smooth and homogeneous, indicating a well intermixed bulk of Si-PCPDTBT and PCBM. The Si-PCPDTBT:C₆₀ThHx and Si-PCPDTBT:C₆₀ThOt layer featured uneven surface morphology with rice-shaped grains. The topography of Si-PCPDTBT:C₆₀ThOt shows an uneven surface with lots of dark hollow features.

The surface of Si-PCPDTBT:PCBM with 1% CN (Fig. 8(d)) is almost identical with the Fig. 8(a). The morphological changes are obvious for the Si-PCPDTBT:C₆₀ThHx and Si-PCPDTBT:C₆₀ThOt layers obtained with 1% CN/dichloroben-

zene. Moreover, their images resemble the distribution and shape in Fig. 8(e) and (f), except the different roughness of 2.73 nm for Si-PCPDTBT:C₆₀ThHx and 3.22 nm for Si-PCPDTBT:C₆₀ThOt. It is worth noting here that the Si-PCPDTBT:PCBM film obtained with the CN additive is smoother and there is no significant change in device performance. However, the additive led to more homogeneous morphology throughout the surfaces of Si-PCPDTBT:C₆₀ThHx and Si-PCPDTBT:C₆₀ThOt, indicating improved J_{sc} , V_{oc} , *FF* and PCEs.

In order to explore the influence of morphology change on the hole and electron charge transport, bipolar FETs were fabricated and subsequently characterized. Measured hole and electron mobility obtained from Si-PCPDTBT:PCBM, Si-PCPDTBT:C₆₀ThHx and Si-PCPDTBT:C₆₀ThOt films with and without CN are summarized in Table 3. Both bipolar FETs using Si-PCPDTBT:PCBM with and without CN showed well balanced hole and electron mobilities. However, because of aggregated nature of C₆₀ThHx and C₆₀ThOt, bipolar FETs using Si-PCPDTBT:C₆₀ThHx and Si-PCPDTBT:C₆₀ThOt without CN exhibited significantly suppressed electron mobilities. For the bipolar FETs using Si-PCPDTBT:C₆₀ThHx and Si-PCPDTBT:C₆₀ThOt with CN, however, electron mobilities were increased, and then it showed balanced hole and electron mobilities. Therefore, we conclude that well mixed homogeneous morphology led balanced charge transport properties, thereby improving solar cell performances.

4. Conclusions

In conclusion, we have investigated the effect of processing additive on fullerene aggregation in polymer BHJ solar cells. New fullerene derivatives, C₆₀ThHx and C₆₀ThOt, bearing a thiophene moiety and alkyl groups were introduced as the acceptor materials. Although C₆₀ThHx and C₆₀ThOt showed quite similar electronic transport properties in OFET, the photovoltaic performances were limited by their aggregative nature. Processing with 1% CN additive, however, changed the aggregated morphology of BHJ films to a smoother and homogeneous morphology, improving photovoltaic performance. This result indicates that processing additive not only influences on polymer side, but also affects fullerene acceptor component.

Acknowledgements

This research at university of Ulsan was supported by Basic Science Research Program (2011-0009148) and

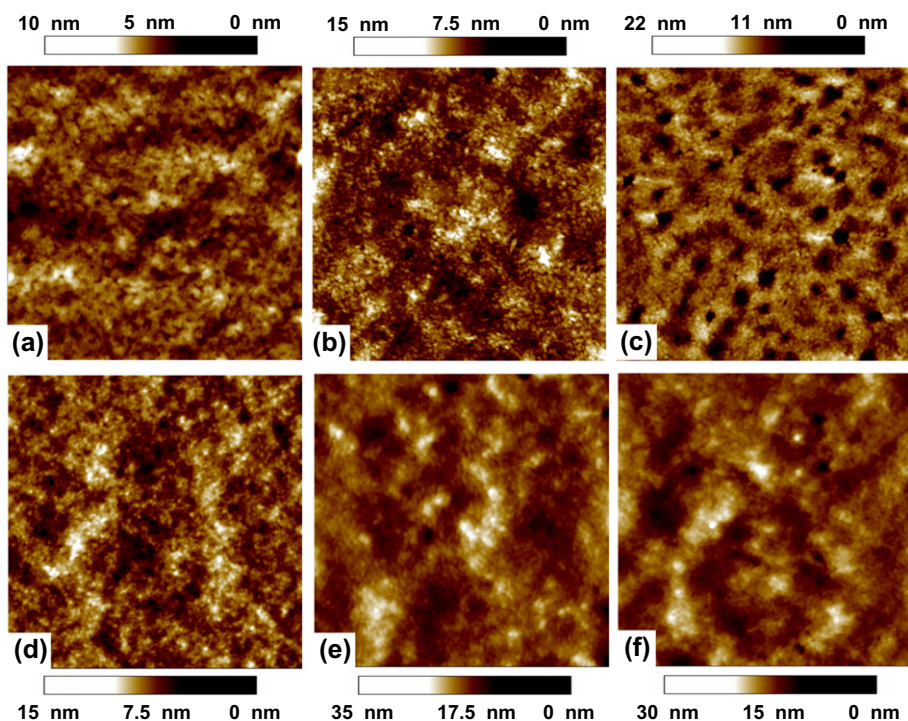


Fig. 8. AFM images ($2\ \mu\text{m} \times 2\ \mu\text{m}$) of (a) Si-PCPDTBT:PCBM, (b) Si-PCPDTBT:C₆₀ThHx, and (c) Si-PCPDTBT:C₆₀ThOt films without the additive. (d)–(f) Corresponding to the (a)–(c) with the 1% CN additive.

Table 3

Hole and electron mobilities obtained from bipolar FETs.

		Hole mobility ($\text{cm}^2\ \text{V s}$)	Electron mobility ($\text{cm}^2\ \text{V s}$)
Si-PCPDTBT:PCBM	Without CN	7.8×10^{-3}	6.4×10^{-3}
	With CN	5.5×10^{-3}	6.1×10^{-3}
Si-PCPDTBT:C ₆₀ ThHx	Without CN	2.1×10^{-3}	4.6×10^{-4}
	With CN	3.2×10^{-3}	2.8×10^{-3}
Si-PCPDTBT:C ₆₀ ThOt	Without CN	1.7×10^{-3}	8.6×10^{-5}
	With CN	8.4×10^{-4}	7.1×10^{-4}

Priority Research Centers Program (2009-0093818) through the National Research Foundation of Korea (NRF) funded by the Ministry of Education, Science and Technology (MEST). JHS thanks a Grant (F0004012-2011-34) from Information Display R&D Center, one of the Knowledge Economy Frontier R&D Program funded by the Ministry of Knowledge Economy of Korean government. All authors thank the NSF (DMR-1121053) for the UPS facility at UCSB. KSL also acknowledges the part of funding support by the Mid-career Researcher Program through an NRF grant funded by the MEST (No. 2011-0000247).

References

- [1] D. Gendron, M. Leclerc, *Energy Environ. Sci.* 4 (2011) 1225.
- [2] C.J. Brabec, S. Gowrisanker, J.J.M. Halls, D. Laird, S. Jia, S.P. Williams, *Adv. Mater.* 22 (2010) 3839.
- [3] A.C. Mayer, S.R. Scully, B.E. Hardin, M.W. Rowell, M.D. McGehee, *Mater. Today* 10 (2007) 28.
- [4] H.-Y. Chen, J. Hou, S. Zhang, Y. Liang, G. Yang, Y. Yang, L. Yu, Y. Wu, G. Li, *Nat. Photonics* 3 (2009) 649.
- [5] H. Ma, H.-L. Yip, F. Huang, A.K.-Y. Jen, *Adv. Funct. Mater.* 20 (2010) 1371.
- [6] L.M. Chen, Z. Xu, Z. Hong, Y. Yang, *J. Mater. Chem.* 20 (2010) 2575.
- [7] J.H. Seo, A. Gutacker, Y. Sun, H. Wu, F. Huang, Y. Cao, U. Scherf, A.J. Heeger, G.C. Bazan, *J. Am. Chem. Soc.* 133 (2011) 8416.
- [8] D. Credgington, R. Hamilton, P. Atienzar, J. Nelson, J.R. Durrant, *Adv. Funct. Mater.* 21 (2011) 2744.
- [9] B. Walker, A.B. Tamayo, X.-D. Dang, P. Zalar, J.H. Seo, A. Garcia, M. Tantiwiwat, T.-Q. Nguyen, *Adv. Funct. Mater.* 19 (2009) 3063.
- [10] G. Li, Y. Yao, H. Yang, V. Shrotriya, G. Yang, Y. Yang, *Adv. Funct. Mater.* 17 (2007) 1636.
- [11] T.-Y. Chu, J. Lu, S. Beaupré, Y. Zhang, J.-R. Pouliot, S. Wakim, J. Zhou, M. Leclerc, Z. Li, J. Ding, Y. Tao, *J. Am. Chem. Soc.* 133 (2011) 4250.
- [12] M.-S. Su, C.-Y. Kuo, M.-C. Yuan, U.-S. Jeng, C.-J. Su, K.-H. Wei, *Adv. Mater.* 23 (2011) 3315.
- [13] J. Peet, J.Y. Kim, N.E. Coates, W.L. Ma, D. Moses, A.J. Heeger, G.C. Bazan, *Nat. Mater.* 6 (2007) 497.
- [14] J.K. Lee, W.L. Ma, C.J. Brabec, J. Yuen, J.S. Moon, J.Y. Kim, K. Lee, G.C. Bazan, A.J. Heeger, *J. Am. Chem. Soc.* 130 (2008) 3619.
- [15] C.V. Hoven, X.-D. Dang, R.C. Coffin, J. Peet, T.-Q. Nguyen, G.C. Bazan, *Adv. Mater.* 22 (2010) E63.
- [16] J.S. Moon, C.J. Takacs, S. Cho, R.C. Coffin, H. Kim, G.C. Bazan, A.J. Heeger, *Nano Lett.* 10 (2010) 4005.
- [17] W. Li, Y. Zhou, B.V. Andersson, L.M. Andersson, Y. Thomann, C. Veit, K. Tvingstedt, R. Qin, Z. Bo, O. Inganäs, U. Würfel, F. Zhang, *Org. Electron.* 12 (2011) 1544.

- [18] H. Kim, J.H. Seo, E.Y. Park, T.-D. Kim, K. Lee, K.-S. Lee, S. Cho, A.J. Heeger, *Appl. Phys. Lett.* 97 (2010) 193309.
- [19] S. Cho, J.H. Seo, K. Lee, A.J. Heeger, *Adv. Funct. Mater.* 19 (2009) 1459.
- [20] S.-H. Oh, S.-I. Na, J. Jo, B. Lim, D. Vak, D.-Y. Kim, *Adv. Funct. Mater.* 20 (2010) 1997.
- [21] Z. He, C. Zhang, X. Xu, L. Zhang, L. Huang, J. Chen, H. Wu, Y. Cao, *Adv. Mater.* 23 (2011) 3086.
- [22] M.C. Scharber, D. Muhlbacher, M. Koppe, P. Denk, C. Waldauf, A.J. Heeger, C.J. Brabec, *Adv. Mater.* 18 (2006) 789.
- [23] P.W.M. Blom, V.D. Mihailetschi, L.J.A. Koster, D.E. Markov, *Adv. Mater.* 19 (2007) 1551.
- [24] M.O. Reese, M.S. White, G. Rumbles, D.S. Ginley, S.E. Shaheen, *Appl. Phys. Lett.* 92 (2008) 053307.